

Radiation-Driven Outflows in Active Galactic Nuclei

Daniel Proga* and Ryuichi Kurosawa*,†

**Department of Physics and Astronomy, University of Nevada Las Vegas, Box 454002,
4505 Maryland Pkwy, Las Vegas, NV 891541-4002*

†*Current Address: Department of Astronomy, Cornell University, Ithaca, NY 14853-6801*

Abstract. We review the results from multi-dimensional, time-dependent simulations of gas dynamics in AGN. We will focus on two types of outflows powered by radiation emitted from the AGN central engine: (i) outflows driven from the innermost part of an accretion disk and (2) outflows driven from a large-scale inflow that is likely the main supplier of material to the central engine. We discuss the relevance of both types of outflows to the so-called AGN feedback problem. However, the AGN feedback should not be considered separately from the AGN physics. Therefore, we also discuss the issue whether the properties of the same outflows are consistent with the gas properties in broad- and narrow-line regions.

Keywords: accretion, accretion – disks – galaxies: jets – galaxies: kinematics and dynamics–
methods: numerical – hydrodynamics

PACS: 95.30.Lz, 98.54.-h, 98.54.Cm, 98.62.Mw, 98.62.Nx

INTRODUCTION

The dynamics of the gas and dust in narrow line regions (NLRs) and broad line regions (BLRs) in active galactic nuclei (AGNs) is driven by gravity but radiation driving can also be important even for sub-Eddington sources (e.g., [1]). Radiation driving can be due to radiation pressure, radiation heating, or both. The radiation force can overcome gravity for sub-Eddington sources when the gas/dust opacity is higher than the electron scattering. The latter is usually used to define the Eddington luminosity, L_{Edd} . The gas opacity can be enhanced by the scattering of photons by UV spectral lines. Radiation pressure on spectral lines (line force) can be significant, provided that the gas is moderately ionized and can interact with the UV continuum through very many UV line transitions. For highly ionized gas, line force is negligible because of a lower concentration of ions capable of providing UV line opacity. In the case of highly or fully ionized gas, an outflow can still be produced if the gas heating is efficient enough for the thermal energy to exceed the gravitational energy.

AGNs with their broad spectral energy distributions (SEDs), are systems where both line driving and radiation heating, in particular X-ray heating, can operate. In fact, a wind driven from an accretion disk by line force is the most promising hydrodynamics (HD) scenario for outflows in AGN, especially high-luminosity quasars. In this scenario, a wind is launched from the disk by the local disk radiation at radii where the disk radiation is mostly emitted in the UV ([2]; [3]). Such a wind is continuous and has a mass-loss rate and velocity that are capable of explaining the blueshifted absorption lines observed in many AGNs, if the ionization state is suitable (e.g., [3]; [4]; [5]). This wind scenario

has a desirable feature, i.e., for the wind motive power it relies on radiation, which is an observable quantity. We note that line-driving can account not only for gross properties of some AGN outflows but also for specific spectral features observed in some quasars ([6];[7]; [8]). However, not all AGN outflows can be explained by line driving because of too low a luminosity, too high an ionization state, or both (e.g., [5]; [9]; [10]). Therefore, other mechanisms such as thermal and magnetic driving are likely also important.

Theoretical models predict that X-ray heating can have profound effects on the gas dynamics in disks. Since X-rays tend to heat low-density gas to a temperature $T_C \sim 10^7$ K, with which matter in an accretion disk is expected to either puff up and form a static corona or produce a thermal wind, depending on whether the thermal velocity exceeds the local escape velocity, v_{esc} (e.g., [11]; [12]; [13]; [14]).

These studies demonstrate that radiation liberated by an accreting disk can drive a powerful outflow from this disk. Therefore one can ask: Can AGN radiation drive an outflow from anywhere other than the disk? If yes, what are the properties of this outflow? In particular, can it explain the properties of BLR and NLR? Can this outflow be a part of AGN feedback? To answer these questions, we recently applied and extended our techniques developed to study disk outflows to model fluid dynamics on scales comparable to the BH's gravitational radius and also on larger scales ([15]; [16]; [17]; [18]; [19]; [20]). In the following, we briefly summarize the main results of our recent work.

SIMULATIONS OF OUTFLOWS FROM INFLOWS

In [15], we calculated a series of models for non-rotating flows that are under the influence of super massive BH gravity and radiation from an accretion disk surrounding the BH. Generally, we used the numerical methods developed by [4]. Our numerical approach allows for the self-consistent determination of whether the flow is gravitationally captured by the BH or driven away by thermal expansion or radiation pressure.

To compute the structure and evolution of inflows/outflows, we solve the equations of HD:

$$\frac{D\rho}{Dt} + \rho \nabla \cdot \mathbf{v} = 0, \quad (1)$$

$$\rho \frac{D\mathbf{v}}{Dt} = -\nabla P - \rho \nabla \Phi + \rho \mathbf{F}^{\text{rad}}, \quad (2)$$

$$\rho \frac{D}{Dt} \left(\frac{e}{\rho} \right) = -P \nabla \cdot \mathbf{v} + \rho \mathcal{L}, \quad (3)$$

where ρ is the mass density, P is the gas pressure, \mathbf{v} is the velocity, e is the internal energy density, \mathcal{L} is the net cooling rate, Φ is the gravitational potential, and \mathbf{F}^{rad} is the total radiation force per unit mass.

In our previous simulations, the total radiation force has two components: one is due to electron scattering, $\mathbf{F}^{\text{rad},e}$ and the other is due to lines $\mathbf{F}^{\text{rad},l}$. The latter can be approximated a modified version of the method developed by [21]. The line force at a point defined by the position vector \mathbf{r} is

$$\mathbf{F}^{rad,l}(\mathbf{r}) = \oint_{\Omega} M(t) \left(\hat{n} \frac{\sigma_e I(\mathbf{r}, \hat{n}) d\Omega}{c} \right) \quad (4)$$

where I is the frequency-integrated continuum intensity in the direction defined by the unit vector \hat{n} , and Ω is the solid angle subtended by the disk and corona at the point. The term in brackets is the electron-scattering radiation force, σ_e is the mass-scattering coefficient for free electrons, and $M(t)$ is the force multiplier – the numerical factor which parametrizes how much spectral lines increase the scattering coefficient. In the Sobolev approximation, $M(t)$ is a function of the optical depth parameter $t = \sigma_e \rho v_{th} / |dv_l/dl|$, where v_{th} is the thermal velocity, and dv_l/dl is the velocity gradient along the line of sight, \hat{n} . The force multiplier approaches zero when all lines become optically thick (i.e., $\lim_{t \rightarrow \infty} M(t) = 0$) and some finite maximum value (M_{max}) when all lines become optically thin (i.e., $\lim_{t \rightarrow 0} M(t) = M_{max}$). The maximum value of the force multiplier is a function of physical parameters of the wind and radiation field, and can be parametrized by the photoionization parameter, ξ . Several studies have shown that M_{max} is roughly a few thousand for gas ionized by a weak or moderate radiation field (e.g., [21]; [22]; [23]; [24]). As the radiation field becomes stronger and the gas becomes more ionized the force multiplier decreases asymptotically to zero (i.e., $\lim_{\xi \rightarrow 0} M_{max} = \text{a few } 10^3$ and $\lim_{\xi \rightarrow \infty} M_{max} = 0$). M_{max} allows us to set a lower limit of the luminosity at which a system can have a “line-driven” wind, [i.e., $L > L_E / (1 + M_{max})$]. We note that using the Castor et al.’s method [21], one can model large scale properties of relatively smooth line-driven winds very well, but cannot capture small scale effects, in particular the so-called line driven instability (e.g., [25]; [26]; [27]).

We adopt an adiabatic equation of state $P = (\gamma - 1)e$, and consider models with the adiabatic index, $\gamma = 5/3$. We performed simulations using the Newtonian potential Φ due to the central BH (the general relativity effects can be neglected because we consider flow dynamics relatively far from the BH). The simulations were performed in spherical polar coordinates assuming axial symmetry about the rotational axis of the accretion disk.

RESULTS

For a $10^8 M_{\odot}$ BH with an accretion luminosity of 0.6 of L_{Edd} , we found that a non-rotating flow settles quickly into a steady state and has two components (1) an equatorial inflow and (2) a bipolar inflow/outflow with the outflow leaving the system along the pole. The first component is a realization of Bondi-like accretion flow. The second component is an example of a non-radial accretion flow becoming an outflow once it is pushed close to the rotational axis of the disk where thermal expansion and radiation pressure can accelerate the flow outward. The main result of these simplified calculations is that the existence of the above two flow components is robust yet their properties are sensitive to the geometry, SED of the radiation field, and the outer boundaries. In particular, the outflow power and the degree of collimation are higher for the model with radiation dominated by UV/disk emission than for the model with radiation dominated by X-ray/central engine emission. This sensitivity is related to the fact that thermal expansion drives a weaker and wider outflow, compared to the radiation pressure.

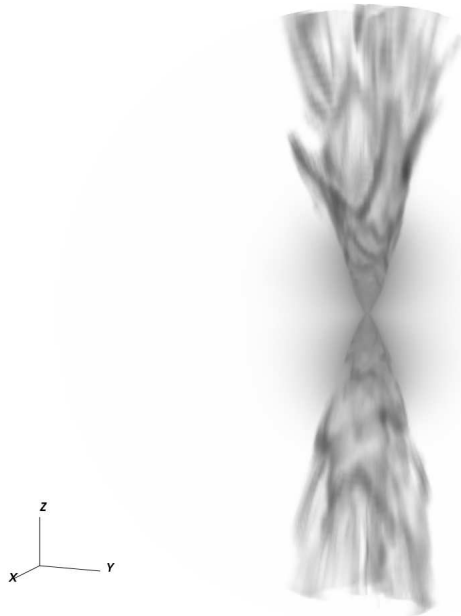


FIGURE 1. Three-dimensional hydrodynamical simulations of outflow formation via redirection of accreting gas by the strong radiation from an accretion disk around a super massive black hole with its mass $M_{\text{BH}} = 10^8 M_{\odot}$. The infalling gas is weakly rotating (sub-Keplerian), and the Eddington ratio of the system is 0.6. The volume rendering representation of the density distributions is shown. The outflow morphology is bi-conical, but the flow contains relatively cold and dense cloud-like structures which resembles those observed in the NRLs of Seyfert galaxies. The figure is from [18].

In [16], we explored effects of gas rotation. As expected, rotation changes the geometry of the flow because the centrifugal force prevents gas from reaching the rotational axis (see fig. 1 in [16]). This, in turn, reduces the mass outflow rate because less gas is pushed toward the polar region. We also found that rotation can lead to fragmentation and time variability of the outflow. As the flow fragments, cold and dense clouds form (figs. 4 and 12 in [16]).

We have also started studying 3-D effects on gas dynamics (e.g., [17]; [18]). In [17], we considered effects of radiation due to a precessing accretion disk on a spherical cloud of gas around the disk. On the other hand, in [18]), we recalculated some models from papers [15] and [16] in full 3-D. Our 3-D simulations of a nonrotating gas show small yet noticeable nonaxisymmetric small-scale features inside the outflow. However, the outflow as a whole and the inflow do not seem to suffer from any large-scale instability. In the rotating case, the nonaxisymmetric features are very prominent¹, especially in the outflow which consists of many cold dense clouds entrained in a smoother hot flow (e.g., see figs. 1 and 2). The 3-D outflow is nonaxisymmetric due to the shear and thermal instabilities. Effects of gas rotations are similar in 2-D and 3-D. In particular, gas rotation increases the outflow thermal energy flux, but reduces the outflow mass and kinetic

¹ Sample movies of the 3-D simulations can be found at http://www.physics.unlv.edu/~rk/research/agn_3d_r

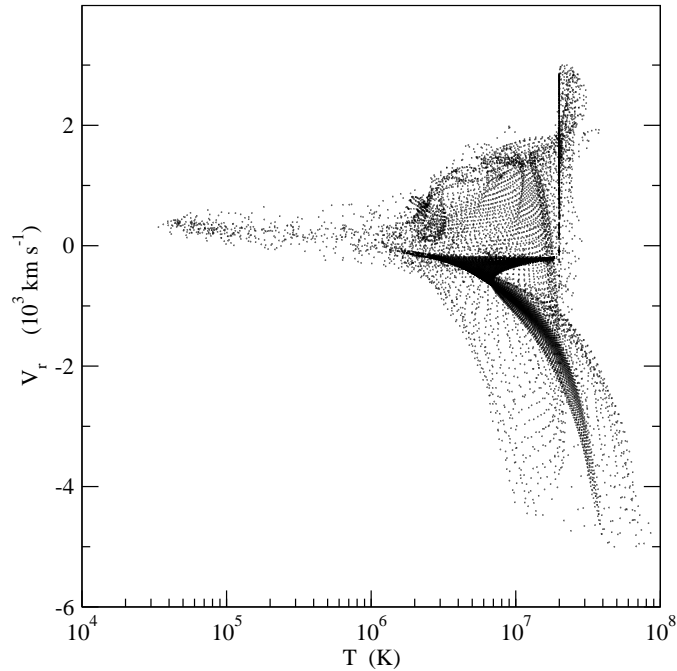


FIGURE 2. A scatter plot of the radial velocity (v_r) versus gas temperature (T) for the model shown in fig. 1. A negative value of v_r indicates an inflow. To avoid overcrowding, only the points on $\phi = 0$ plane are shown. A large fraction of gas is in outflow motion ($v_r > 0$) for the models with rotation and a wide range of the temperature is associated with the outflowing gas. The figure is from [18].

energy fluxes. In addition, rotation leads to time variability and fragmentation of the outflow in the radial and latitudinal directions. The collimation of the outflow is reduced in the models with gas rotation. The main different effect of rotation in 3-D compared to 2-D is that the time variability in the mass and energy fluxes is reduced in the 3-D case because of the outflow fragmentation in the azimuthal direction.

Our recent simulations, demonstrate that AGNs can have a substantial outflow originating from the infalling gas. Such an outflow can reduce the rate at which matter is supplied to the central region of AGN because its mass loss rate can be significantly higher than the mass inflow rate at small radii (see fig. 3). For example, as little as 10% of the inflow at large radii can reach small radii because 90% of the inflow is turned into an outflow. In general, the kinetic power dominates the thermal power at all radii in both models with and without gas rotation; however, the thermal power contribution is non-negligible in the models with gas rotation (fig. 3). The X-ray heating becomes more effective in the rotating gas environment because the flows become more non-radial and will be subjected to the direct exposure to the strong radiation from central continuum radiation source.

In [19], the radiation-driven AGN outflow model of [15] is extended by relaxing the assumption of a constant accretion luminosity. This allows us to determine the accretion luminosity consistently with the mass accretion rate at the inner boundary, and consequently the two quantities are coupled through the radiation field. This is an improvement toward a more comprehensive self-consistent hydrodynamical models with radia-

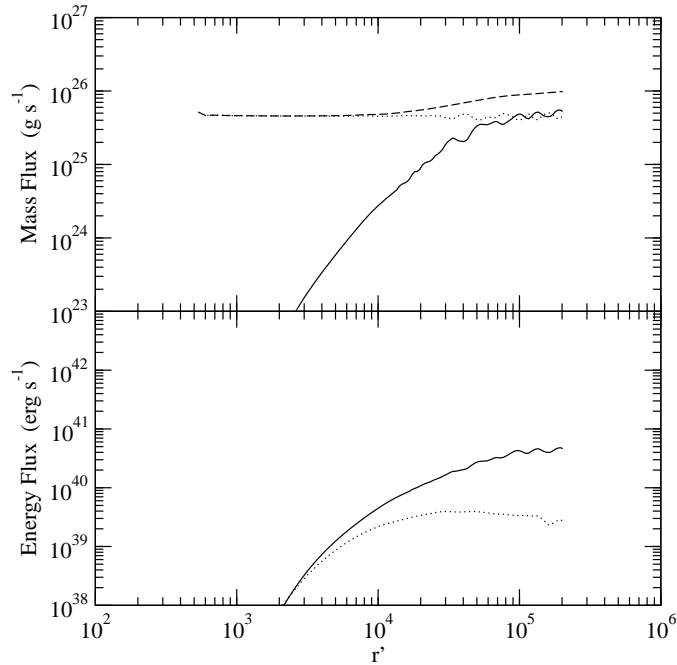


FIGURE 3. Mass and energy fluxes as a function of radius for the model shown in fig. 1. The panel is subdivided into two parts: *top* (mass flux) and *bottom* (energy flux). In the mass flux plot, the inflow (*dashed line*; \dot{M}_{in}), outflow (*solid line*; \dot{M}_{o}) and net (*dotted lines*; \dot{M}_{net}) mass fluxes, are separately plotted, as a function of radius. The absolute values of \dot{M}_{in} and \dot{M}_{net} are plotted here since they are negative at all radii. The length scale is in units of the inner disk radius ($r' = r/r_*$ where $r_* = 8.8 \times 10^{13}$ cm). In the energy flux plots, the kinetic energy (*solid line*) and the thermal energy (*dotted line*) fluxes are shown. The figure is from [18].

tive feedback. For the models with high temperature gas at large radii (~ 10 pc) and high luminosities, we find a strong correlation between the mass-outflow rate (\dot{M}_{out}) and the luminosity (L). The power law index (q) describing the $\dot{M}_{\text{out}}-L$ relation is $q = 2.0 (\pm 0.1)$, which is very similar to that for radiation-driven stellar and disk wind models. More surprisingly, for high density at large radii, we find steady state solutions with the accretion luminosity *exceeding* the Eddington limit. The super-Eddington accretion proceeds in the equatorial region and is possible because the radiation flux from the disk is significantly reduced in the equatorial direction due to the geometrical foreshortening effect² (see fig. 4).

Based on a set of axisymmetric simulations presented in [19], we analyzed the energy, momentum, and mass feedback efficiencies due to radiation from AGN (see [20]). We find that even for the strongest outflow, the ratio between the outflow kinetic power and the radiation power is very low ($\sim 10^{-4}$ at the peak; see fig. 5). One of the reasons for this relatively low efficiency of the large scale outflows is that for large densities at large radii, accretion proceeds in the equatorial region, and the radiation flux from the disc is significantly reduced the geometrical foreshortening effect, as also mentioned above.

² Sample movies of the 2-D simulations can be found at http://www.physics.unlv.edu/~rk/research/agn2d_su

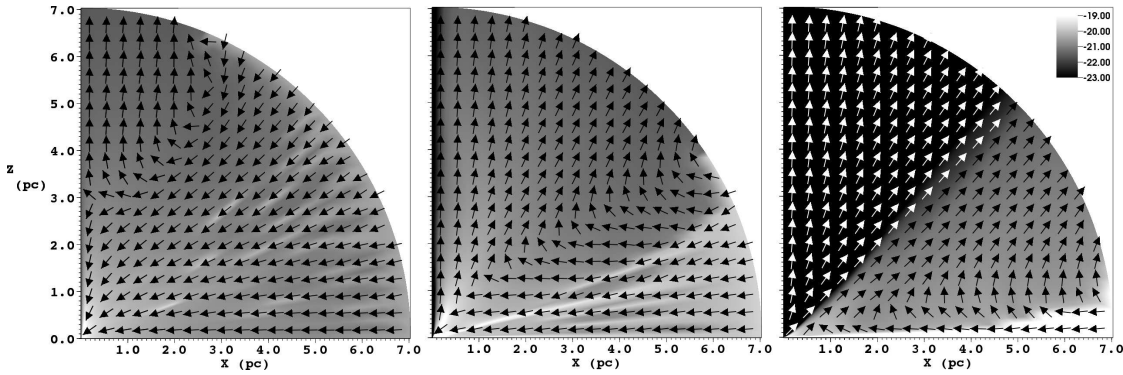


FIGURE 4. Examples of the density and velocity maps from a set of two-dimensional simulations (without the temperature constrained at the outer boundary) presented in [19]. The density (in logarithmic scale) is over-plotted with the directions of poloidal velocity as arrows. The figures are placed in order of increasing density at the outer boundaries (ρ_o) from the left to right. The self-consistently determined accretion luminosities (in the unit of Eddington luminosity) are $\Gamma = 0.32, 0.71$ and 4.3 , from the left to right panels. For the low density (ρ_o) and low accretion luminosity model (*left panel*), the outflow is very narrow ($0^\circ \lesssim \theta \lesssim 30^\circ$), and the inflow is very wide ($30^\circ \lesssim \theta \lesssim 90^\circ$). As the density (ρ_o) and accretion luminosity increase (*middle panel*), the outflow becomes wider ($0^\circ \lesssim \theta \lesssim 50^\circ$), whereas the inflow becomes narrower ($50^\circ \lesssim \theta \lesssim 90^\circ$). For the very high density and accretion model (*right panel*), the outflow occurs over a very wide range of the polar angle ($0^\circ \lesssim \theta \lesssim 85^\circ$), and the accretion region is now confined to a thin equatorial wedge (the disk-wind-like solution). The figures are from [20].

The coupling between the radiation and matter becomes less efficient once the inflow-outflow morphology becomes the “disk wind like” (the right panel in fig. 4) because of the “mismatch” between the direction in which the disk radiation peaks (in the polar direction) and the direction of the matter inflow (in the equatorial direction).

Compared to the energy (thermal only) feedback efficiencies ~ 0.05 required in the recent cosmological and galaxy mergers simulations (e.g., [28]; [29]; [30]; [31]; [32]), our thermal energy feedback efficiency at the peak value is about 5×10^3 times smaller. Our total and kinetic energy efficiencies are about 5×10^2 times smaller than the value required in cosmological simulations. These large discrepancies might indicate a few things. For example, our models are missing important elements. In particular, we do not include effects of dust which could make the outflows much stronger.

On the other hand, it is also possible that the AGN feedback may not be as effective as one might have had expected. Instead, other forms of feedback may be more significant than the AGN feedback via radiation on scales between 10^{-2} and a few parsecs. For example, the feedback via supernovae, star formation processes, the strong stellar wind from massive stars, and strong accretion disk winds (discussed in section 1) or jets from AGN may play more important roles. The last two forms of the feedback require a proper treatment of magnetic field, as they may carry a significant fraction of the total outward flux in energy and momentum.

Finally, the AGN feedback efficiency may be indeed low, and the AGNs take a long time to influence their environment. We note that in our models the AGNs do not shut off the mass supply completely even at very high luminosities ($\Gamma \gtrsim 1$). This indicates that the AGNs can operate on a very long time scale over which their affects can accumulate, and eventually become significant.

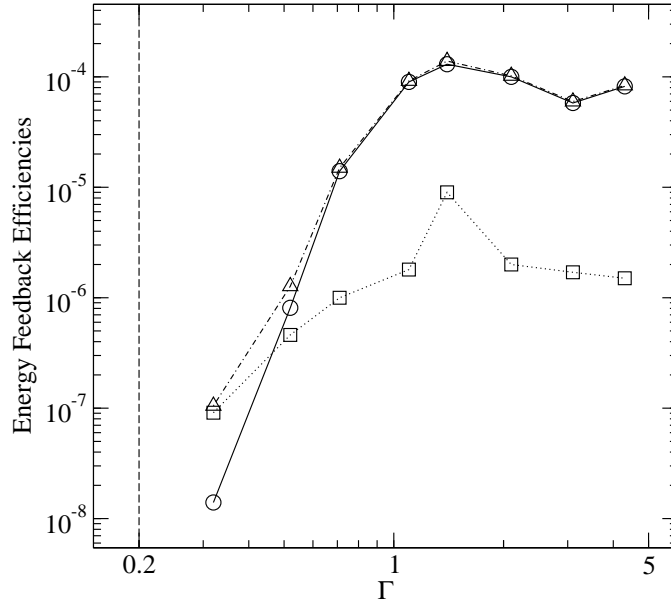


FIGURE 5. The efficiencies of converting the black hole accretion luminosity L_a to the rate of energy deposition to the surrounding gas plotted as a function of the Eddington ratio (Γ). The values are based on the 2-D simulations similar to those shown in fig. 4. The kinetic energy feedback efficiency ϵ_k (circles), the thermal energy feedback efficiency ϵ_{th} (squares) and the total energy feedback efficiency $\epsilon_t = \epsilon_k + \epsilon_{th}$ (triangles) are shown separately. The maximum total energy feedback efficiency is $\sim 10^{-4}$. For the models with relatively low Eddington ratio ($\Gamma \lesssim 0.4$), the thermal feedback is more efficient than the kinetic feedback ($\epsilon_{th} > \epsilon_k$). For the models with relatively high Eddington ratio ($\Gamma \gtrsim 0.6$), the kinetic feedback is more efficient than the thermal feedback by a factor of ~ 10 to ~ 100 . The model with $\Gamma = 0.2$ does not form an outflow, and the vertical line (dashed) at $\Gamma = 0.2$ indicates an approximate Γ value below which no outflow forms. The flattening of the efficiencies beyond $\Gamma \approx 1$ is caused by the transition of the inflow-outflow morphology to a “disk wind like” configuration for the larger Γ models (c.f., fig. 4). The figure is from [20].

CONCLUSIONS

The main conclusions from our recent simulations of radiation driven large scale outflows in AGN include:

- A significant fraction of the inflowing matter can be expelled by radiation heating and pressure.
- The non-rotating flow settles into a steady inflow/outflow solution. Rotation of the flow and large optical depth lead to time variability in the inflow/outflow solution.
- In the time variable flows, dense clouds form. This could be applicable to NLR in AGN.
- The large outflows are multi-temperature/phase and could explain warm absorbers in AGN.
- The mass supply rate does not appear to be limited by the AGN radiation.
- The large-scale outflows are efficient in removing matter but inefficient in carrying out energy.

- Radiation drives much more powerful outflows from small scales than from large scales.

ACKNOWLEDGMENTS

This work was supported by NASA through grant HST-AR-11276 from the Space Telescope Science Institute, which is operated by the Association of Universities for Research in Astronomy, Inc., under NASA contract NAS5-26555.

REFERENCES

1. J. H. Krolik, *Active galactic nuclei : from the central black hole to the galactic environment*, Princeton, N. J. : Princeton University Press, 1999.
2. I. Shlosman, P. A. Vitello, and G. Shaviv, *ApJ* **294**, 96–105 (1985).
3. N. Murray, J. Chiang, S. A. Grossman, and G. M. Voit, *ApJ* **451**, 498 (1995).
4. D. Proga, J. M. Stone, and T. R. Kallman, *ApJ* **543**, 686–696 (2000).
5. D. Proga, and T. R. Kallman, *ApJ* **616**, 688–695 (2004).
6. N. Arav, and M. C. Begelman, *ApJ* **434**, 479–483 (1994).
7. N. Arav, K. T. Korista, T. A. Barlow, and Begelman, *Nature* **376**, 576–578 (1995).
8. N. Arav, *ApJ* **465**, 617–630 (1996).
9. D. Chelouche, and H. Netzer, *ApJ* **625**, 95–107 (2005).
10. S. B. Kraemer, I. M. George, D. M. Crenshaw, J. R. Gabel, T. J. Turner, T. R. Gull, J. B. Hutchings, G. A. Kriss, R. F. Mushotzky, H. Netzer, B. M. Peterson, and E. Behar, *ApJ* **633**, 693–705 (2005).
11. M. C. Begelman, C. F. McKee, and G. A. Shields, *ApJ* **271**, 70–88 (1983).
12. E. C. Ostriker, C. F. McKee, and R. I. Klein, *ApJ* **377**, 593–611 (1991).
13. D. T. Woods, R. I. Klein, J. I. Castor, C. F. McKee, and J. B. Bell, *ApJ* **461**, 767 (1996).
14. D. Proga, T. R. Kallman, J. E. Drew, and L. E. Hartley, *ApJ* **572**, 382–391 (2002).
15. D. Proga, *ApJ* **661**, 693–702 (2007).
16. D. Proga, J. P. Ostriker, and R. Kurosawa, *ApJ* **676**, 101–112 (2008).
17. R. Kurosawa, and D. Proga, *ApJ* **674**, 97–110 (2008).
18. R. Kurosawa, and D. Proga, *ApJ* **693**, 1929–1945 (2009).
19. R. Kurosawa, and D. Proga, *MNRAS* **397**, 1791–1803 (2009).
20. R. Kurosawa, D. Proga, and K. Nagamine, *ArXiv e-prints* (2009), 0906.3739.
21. J. I. Castor, D. C. Abbott, and R. I. Klein, *ApJ* **195**, 157–174 (1975).
22. D. C. Abbott, *ApJ* **259**, 282–301 (1982).
23. I. R. Stevens, and T. R. Kallman, *ApJ* **365**, 321–331 (1990).
24. K. G. Gayley, *ApJ* **454**, 410–419 (1995).
25. L. B. Lucy, and P. M. Solomon, *ApJ* **159**, 879–893 (1970).
26. S. P. Owocki, and G. B. Rybicki, *ApJ* **284**, 337–350 (1984).
27. S. P. Owocki, J. I. Castor, and G. B. Rybicki, *ApJ* **335**, 914–930 (1988).
28. V. Springel, T. Di Matteo, and L. Hernquist, *MNRAS* **361**, 776–794 (2005).
29. B. Robertson, L. Hernquist, T. J. Cox, T. Di Matteo, P. F. Hopkins, P. Martini, and V. Springel, *ApJ* **641**, 90–102 (2006).
30. D. Sijacki, V. Springel, T. di Matteo, and L. Hernquist, *MNRAS* **380**, 877–900 (2007).
31. T. Di Matteo, V. Springel, and L. Hernquist, *Nature* **433**, 604–607 (2005).
32. P. H. Johansson, T. Naab, and A. Burkert, *ApJ* **690**, 802–821 (2009).